

# Improving identification of weak spectral lines in the presence of a strong continuum

Eyal Schwartz<sup>1,2</sup> · Stephen G. Lipson<sup>1</sup> · Erez N. Ribak<sup>1</sup>

Received: 10 November 2015 / Accepted: 4 April 2016  
© Springer Science+Business Media Dordrecht

**Abstract** Observing faint spectral signals from light sources in the presence of an overwhelming background is a common goal in many aspects of physics and astronomy. By using an optimized selected part of a Fourier interferogram, we demonstrate that observability of such faint signals can be much improved. We present astronomical observations, in an on-sky experiment, made on several spectral types of star using a breadboard common path scanless interferometer on the Wise Observatory 1m telescope. We obtain an improvement of signal-to-background of up to 35 for a given exposure time.

**Keywords** Technique: interferometers · Methods: observational, data analysis · Instrumentation: interferometers, spectroscopic

## 1 Introduction

The detection and analysis of spectra in the settings of a laboratory or the outside world are of the highest importance in many scopes of science in general, and physics in particular. Moreover, most of our knowledge of the universe at large is provided by analyzing the complex spectra of objects that we cannot resolve. It is a fundamental corner stone in the research of countless phenomena in nature, such as the dynamics of stellar and galactic objects, atmospheric sounding, trace gases and even neuroscience (Hearnshaw

1986; Rodgers 2000; Grieco et al. 2011; Ferrari et al. 1985). Following that, one of the main obstacles in observational astronomy overall, and specifically in extra-solar objects, is the detection of faint spectral signals in the presence of an overpowering background light source, which arises in many interesting scenarios where the specific wavelengths of the spectra are unknown. For example, the luminosity ratio between a bright Sun-like star and a small, as well as faint, habitable Earth-like exoplanet (i.e. extra-solar planet) could be up to  $10^{10}$  in the visible range of the spectrum and  $10^6$  in the mid-IR. Therefore, detecting any spectral features originating from such an exoplanet in the combined light collected, even by the largest active telescopes today, is yet to be achieved. Moreover, when searching for signatures of complex molecules (such as chlorophyll variants) which have evolved differently from those on Earth, the exact wavelengths might be unknown. The relevant quantity to be optimized is the observability, or line contrast, of a spectral feature, which is the signal depth or peak (absorption or emission line) compared to the average background flux level (Lovis and Fischer 2010), i.e. Signal/Background.

In a recent paper (Schwartz et al. 2012) we suggested a method of improving the observability(contrast) of faint spectral lines in the presence of a strong background using an adaptation of Fourier spectroscopy. The method involves using an off-center region of the Fourier interferogram optimized for the width of the spectral lines in question. Furthermore, it is equally applicable to both absorption and emission lines, which can often be masked by scattering from a strong background. The above-mentioned paper presented the basic physics of this method with an analytical estimation of the signal-to-noise level, supported by simulations which included photon noise, and it was suggested for exoplanet detection and analysis.

✉ E. Schwartz  
eyal.schwartz@otago.ac.nz

<sup>1</sup> Physics Department, Technion—Israel Institute of Technology, Haifa, 32000, Israel

<sup>2</sup> Present address: Physics Department, University of Otago, Dunedin, 9016, New Zealand

Fourier spectroscopy is a measurement technique whereby the temporal auto-correlation function of light is measured using an interferometer in which the signal is interfered with itself after a time delay. This is most commonly done using a Michelson interferometer, although other interferometers can be used for the same purpose. The time delay is introduced using an optical path difference (OPD) (Bell 1972; Lipson et al. 2011).

In Fourier transform spectroscopy, the spectrum,  $S(k)$  ( $k$  is the wavenumber), and the interferogram,  $I(\Delta)$  ( $\Delta$  is the OPD), constitute a Fourier pair defined by the following equations,

$$S(k) = \int_{-\infty}^{+\infty} I(\Delta) e^{-2\pi i k \Delta} d\Delta, \quad (1)$$

$$I(\Delta) = \int_{-\infty}^{+\infty} S(k) e^{2\pi i k \Delta} dk. \quad (2)$$

The spectrum and the interferogram are, in practice, band-limited functions; therefore, taking into account that the interferogram is sampled in a range of optical path differences,  $\Delta_l$  to  $\Delta_h$ , we modify (1) by introducing the data-sampling window,  $W(\Delta)$ , such that

$$S_f(k) = \int_{-\infty}^{+\infty} W(\Delta) I(\Delta) e^{-2\pi i k \Delta} d\Delta \quad (3)$$

where

$$W(\Delta) = \begin{cases} 1 & \Delta_l \leq |\Delta| \leq \Delta_h, \\ 0 & \text{Otherwise.} \end{cases} \quad (4)$$

The Fourier transform of this window function is the difference of two sinc functions,

$$\tilde{W}(k) = 2[\Delta_h \text{sinc}(2\pi k \Delta_h) - \Delta_l \text{sinc}(2\pi k \Delta_l)]. \quad (5)$$

Therefore, after convolution with the full spectrum,  $S(k)$ , we get the band-pass filtered spectrum,  $S_f(k)$ . This description is very similar to partial temporal scanning of one side of a classical Fourier interferometer, and is very extensively described by Grieco et al. (2011). The major difference is that we take a long exposure image of the fringes, instead of scanning them in front of the detector.

The presented method in this work is based on the principle that a spectral feature with typical width  $\delta k$  contributes most of its power into a region of path length of order of  $1/\delta k$  in the interferogram. As a result, both broader and narrower features can be attenuated by choosing an appropriate region of path lengths, thus allowing fainter features to be better seen. We should point out that limiting the path difference range necessarily reduces the spectral resolution. However, the observability of the features with the designated line-width is substantially improved, even when compared with the grating spectrometer data.

In this work we present an implementation of this idea in an on-sky experiment, and conduct a set of astronomical observations on several spectral types of star where we have been able to improve the observability (Signal/Background), i.e. contrast (Lovis and Fischer 2010), of known spectral features. In these observations we show a major improvement in the observability of the Balmer series and neutral helium absorption lines present in the spectrum of hot stars. Compared to the spectrum obtained in the usual manner of Fourier spectroscopy, the improvement achieved was up to a factor of 35. We further compare the observability of these spectral lines with results from a conventional grating spectrometer under the same observational conditions. We have also been able to detect spectral details (such as Mg I, TiO and ZrO) for the cooler stars which were masked by stronger features in their spectra. An advantage of the Fourier method we present compared to a grating spectrometer is that it is not necessary to measure the whole spectral band and we only estimate the widths of spectral features in question. These results indicate that the method could contribute to different fields of observational astronomy, such as exoplanet spectral analysis and spectroscopy of Active Galactic Nuclei (AGN), as well as other low-contrast spectral measurements in other fields of physics.

The partially scanned interferogram method was developed many years ago (Kyle 1977) and has been implemented in the IASI satellite which uses this principle to measure atmospheric CO<sub>2</sub> lines by temporal scanning with a Michelson interferometer (Grieco et al. 2011). Nevertheless, when the Fourier interferogram is recorded as the path difference changes with time, atmospheric turbulence and vibrations cause intensity fluctuations which have to be taken into consideration when analyzing the data. More losses are caused by the use of slit or fiber optics input. Moreover, the scanning spans the full interferogram while the post analysis is done only on the relevant parts.

For the purpose of our observations, we used a nearly-common-path white light, scanless and slitless interferometer originally designed for spatial coherence measurements of stellar objects (Ribak and Lipson 1981; Ribak and Leibowitz 1985; Ribak et al. 1985; Ribak 2006; Schwartz 2014), shown schematically in Fig. 1. This was a breadboard prototype system constructed in order to test the presented concept without any engineering optimization. In this setup, we exploit the two complementary interferometric output channels thus using all of the light collected.

The interferometer we employed is made of two beam splitters, where one splits the light into two beams and the other splits each beam again, while combining them into two pairs of coaxial beams. Thus we get two complementary images of the aperture, with a flat single fringe across them. To increase the fringe density, we rotate slightly the second beam splitter, creating an angle between the wave fronts.

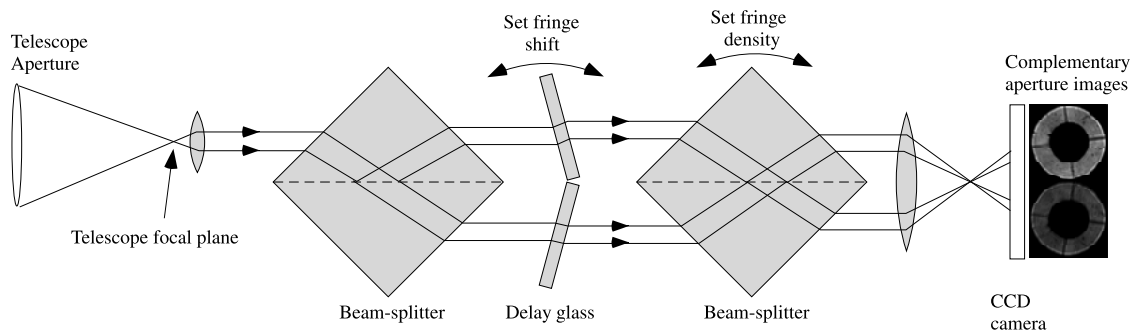
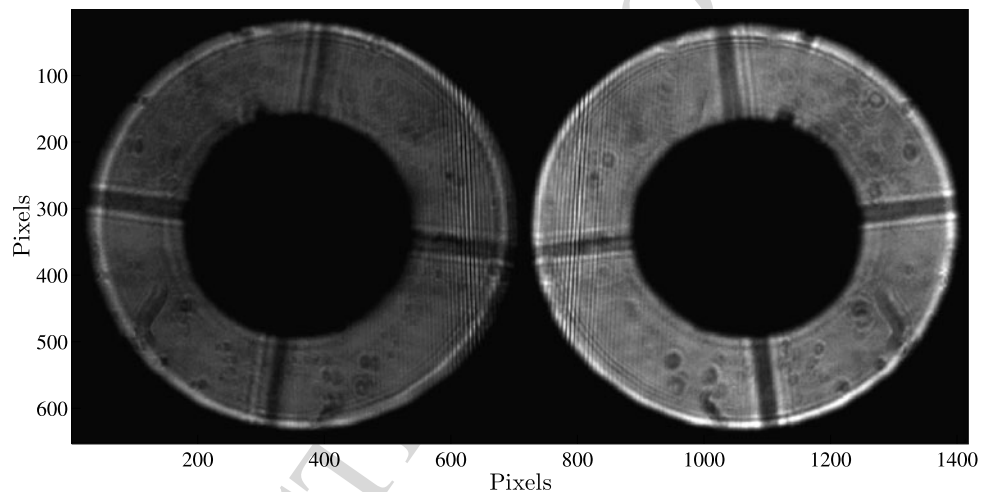


**Fig. 1** Schematics of the zero-shear interferometer used in observations. The positions of the delay glasses and of the beam-splitter are set before the observation

**Fig. 2** Complementary channels of the interferometer for the Mira variable S-type star R Andromedae



Thus each position across the fringes corresponds to a different path delay, equivalent to a temporal change in traditional Fourier transform interferometers. To have an optical path difference between the two beams, we rotate a stage holding two angled flat glasses, adding path to one beam while reducing it at the other beam. Thus the central (black and white) fringe is shifted out of the aperture. The path difference between the glasses might cause secondary dispersion effects, which can be easily removed in the calibration process. This was confirmed on a laboratory calibration source with a known spectrum. Hence, what remains on the aperture is a fixed set of fringes, which is recorded by a cooled CCD camera, corresponding to the required range of path-difference values, and therefore saving the need for temporal scanning of the fringes.

The fringe pattern is then integrated as long as necessary to achieve the required signal to background ratio (S/B), without needing correction for fringe jitter. This way the whole exposure time is devoted to the region of interferometric path difference of interest. It is possible to produce another side band by setting an opposite delay, but since the spectrum is a real function with no phase, this would add no further information and waste valuable limited observation

time. Once the path difference is set, it is extremely stable against vibrations, winds and thermal effects, owing to the beams' proximity, their parallelism between the beam splitters, and the compact and enclosed volume of the interferometer. Furthermore, we utilized the apparatus at zero shear, hence gaining the advantage of insensitivity to the size of the observed object and to atmospheric turbulence.

Figures 2 and 3 show examples of interferogram images from the stars R Andromedae, integrated for 200 seconds, and from Betelgeuse integrated for 3 seconds.

In Fig. 3, we show the interference fringes in greater detail. In this example, only the selected part of the interferogram is in the field of view which shows that fainter and more delicate fringe patterns are revealed when concentrating the exposure time on this part of the interferogram.

## 2 Observations

We conducted a series of observations using the Wise Observatory 1m telescope for which we chose a sample of standard stars of different spectral type and magnitude as shown in Table 1. We installed the common-path interferometer described above and used it to obtain the interferograms of

**Table 1** List of astronomical objects observed with magnitude in the visual range, spectral type and effective temperature (Schiller and Przybilla 2008; Kovtyukh et al. 2003; Kervella 2004; Keenan et al. 1954; Thomas 2005; Valenti 1998; Stone 1977; Jacoby et al. 1984; Pecaut and Mamajek 2013)

Star	Spectral type	$m_v$	$T_{eff}$ [°K]
BD+25°3491(Spec. Std.)	B1.5V	10.47	24800
Deneb ( $\alpha$ Cygni)	A2Ia	1.25	8525
Procyon A ( $\alpha$ Canis Minoris)	F5IV-V	0.34	6530
16 Cygni A	G1.5Vb	5.96	5803
Aldebaran ( $\alpha$ Tauri)	K5III	0.86	3910
Betelgeuse ( $\alpha$ Orionis)	M2Iab	0.42	3600
R Andromedae	S6/4.5e (Mira variable)	7.39	2000–3500

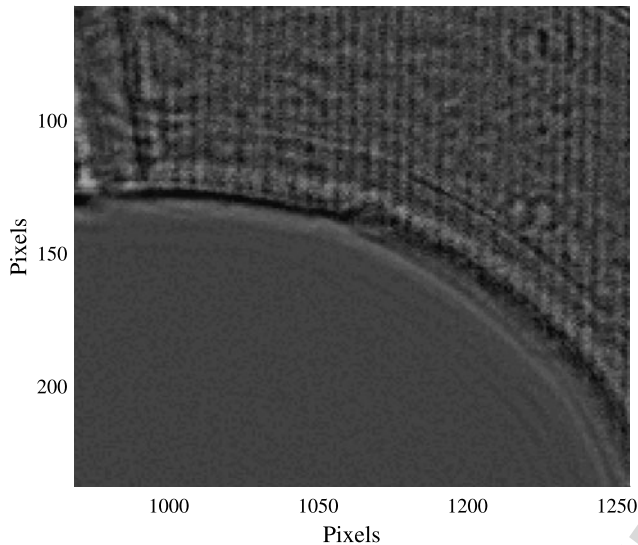


**Fig. 3** Magnified image of the difference between complementary channels for the star Betelgeuse, which removes most of the background image of the telescope aperture. The selected part of the interferogram shows that fainter and more delicate fringe patterns are revealed when adjusting the exposure time for this part of the interferogram

each star. We then retrieved their spectra by Fourier analysis of the interferogram, after using several sources of known wavelengths (B–R bands) to calibrate the instrument. The interferograms were recorded during exposure times ranging between a few seconds to several hundreds of seconds in order to maintain an adequate S/B.

For each observational target, we first recorded the full interferogram (i.e. starting from zero path difference) then added a constant path difference, and recorded the selected part corresponding to the spectral line width in question in order to maximize its S/B. In the first three examples we focused on the prominent Balmer series of hydrogen lines (A, F & G type) (Kramida et al. 2013), while for the latter (B, K, M & S type) we chose spectral lines such as Na I, Mg I and different molecular structures (Baxandall 1924; Jacoby et al. 1984).

In order to estimate the path differences required for maximum sensitivity to the spectral widths in question, we first

derived a model of the contributions to the interferogram from the spectral lines widths based on a Gaussian profile. Following (1), (2), the actual recorded interferogram is  $I(\Delta) = I_0 + I_M(\Delta)$  where  $I_0$  is the mean intensity background and  $I_M(\Delta)$  is the modulated part of the interferogram which consists of the spectral information. Assuming the source spectrum is a Gaussian of unit maximum value with central wavenumber  $k_0 = 2\pi/\lambda_0$  ( $\lambda_0$  is the central wavelength of the spectral line) and a typical width  $\delta k_0$ , i.e.

$$S(k) = e^{-\frac{(k-k_0)^2}{2(\delta k_0)^2}}, \tag{6}$$

then the modulated part of interferogram,  $I_M(\Delta)$ , is the real part of the Fourier transform (or simply the cosine transform) of  $S(k)$ ,

$$I_M(\Delta) = \sqrt{2\pi} \delta k_0 \cos(k_0 \Delta) e^{-\frac{\Delta^2 (\delta k_0)^2}{2}}. \tag{7}$$

We judge the information,  $H$ , in the interferogram as the RMS, i.e.  $\sqrt{\langle I_M^2(\Delta) \rangle}$ , where the average is evaluated in the scanned part of the interferogram,  $[\Delta_l, \Delta_h]$ , thus giving,

$$H = \frac{\pi}{2} \delta k_0 \int_{\Delta_l}^{\Delta_h} e^{-\frac{\Delta^2 (\delta k_0)^2}{2}} d\Delta. \tag{8}$$

Evaluating the Gaussian integral gives,

$$H = \frac{\pi}{2} \left[ \operatorname{erf}\left(\frac{\delta k_0 \Delta_h}{\sqrt{2}}\right) - \operatorname{erf}\left(\frac{\delta k_0 \Delta_l}{\sqrt{2}}\right) \right]. \tag{9}$$

Next, we approximated numerically the information content (line contrast),  $H$  (9) for different spectral line widths  $\delta k_0$  and path differences,  $[\Delta_l, \Delta_h]$ . In Fig. 4. we present four examples of  $H$  (normalized by  $\pi/2$ ) for various path difference ranges as we flip through the range of line widths,  $\delta k_0$ . Firstly, Example 1 is the case of full interferogram  $[\Delta_l, \Delta_h] = 0 \mu\text{m} - 150 \mu\text{m}$ . Secondly, Example 2 is the case of a partial interferogram including both narrow and broad features with  $[\Delta_l, \Delta_h] = 15 \mu\text{m} - 150 \mu\text{m}$ . Thirdly, Example 3 is the case of a band pass partial interferogram sensitive mostly to broad spectral features at the range  $[\Delta_l, \Delta_h] =$

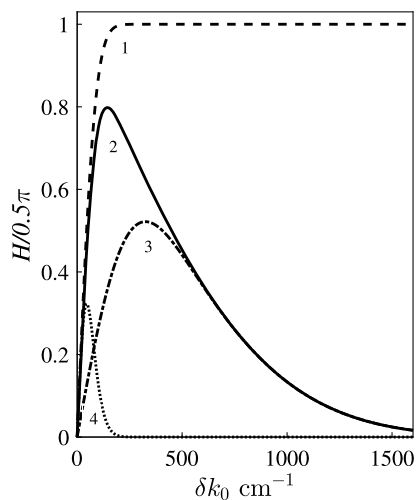


**Fig. 4** The information,  $H$  (normalized by  $\pi/2$ ), stored in the interferogram (9) vs. different spectral line widths,  $\delta k_0$  for the cases of: 1. full interferogram, OPD = [0  $\mu\text{m}$ , 150  $\mu\text{m}$ ], 2. partial interferogram, OPD = [15  $\mu\text{m}$ , 150  $\mu\text{m}$ ], 3. broad band pass—partial interferogram, OPD = [15  $\mu\text{m}$ , 50  $\mu\text{m}$ ], 4. narrow band—pass partial interferogram, OPD = [150  $\mu\text{m}$ , 300  $\mu\text{m}$ ]

15  $\mu\text{m}$ –50  $\mu\text{m}$ . Finally, Example 4. is the case of narrow band pass partial interferogram [ $\Delta_l$ ,  $\Delta_h$ ] = 150  $\mu\text{m}$ –300  $\mu\text{m}$ .

It is important to notice from Fig. 4. that when we include the zero path difference (full interferogram—Example 1) there is no peak sensitivity, and  $H$  approaches a constant as  $\delta k_0$  gets larger as expected when you include a continuum contribution to the interferogram. By choosing the OPD appropriately, we conform our sensitivity for the  $\delta k_0$  of the expected spectral features.

Following this, we attempted to estimate the optimal path difference range needed for all the spectral lines, which resulted in a span of OPDs' of 5  $\mu\text{m}$  to 300  $\mu\text{m}$  for the various line widths. Therefore, from (9) we got that the peak sensitivity to the different widths in the interferogram ranges to be  $\delta k_0 \sim 35$ –200  $\text{cm}^{-1}$ .

In practice, for the actual observations, the spectrum deviated from our Gaussian profile model and we found that the best sensitivity was with a variety of ranges of path differences (from broad features band pass to narrower ones) that spans from 6  $\mu\text{m}$  to as long as 280  $\mu\text{m}$ . Furthermore, as an example, in a case of OPD range of 6  $\mu\text{m}$ –110  $\mu\text{m}$  spectral details broader than  $\delta k = (6 \mu\text{m})^{-1} \approx 1700 \text{ cm}^{-1}$  would be wiped out (e.g. black body continuum). The best improvement would be to spectral details with typical width of (maximum path difference) $^{-1} = (110 \mu\text{m})^{-1} \approx 90 \text{ cm}^{-1}$ , while higher-resolution features, with  $\delta k$  much less than this, would be attenuated by a factor of  $\sim \delta k/50 \text{ cm}^{-1}$  because only this fraction of their interferogram would be sampled up to 110  $\mu\text{m}$ . Furthermore, in this example, the optimum band-width, 90  $\text{cm}^{-1}$  would translate at the wavelength range of 4000  $\text{\AA}$ –8000  $\text{\AA}$  to spectral

line widths of  $\delta\lambda = 15 \text{ \AA}$ –60  $\text{\AA}$ . It is important to notice that spectral line widths are known to vary quite significantly due to different stellar dynamics (Jaschek and Jaschek 1995). The typical average line widths presented in this work were estimated to span from 4  $\text{\AA}$  to 32  $\text{\AA}$  (Chesneau et al. 2010; Kaufer et al. 1996; Schiller and Przybilla 2008; Prieto et al. 2002; Perrin and Spite 1981; Hardorp and Tomkin 1983; Kaler 1989; Montes et al. 1999; Saad and Nouh 2011).

## 2.1 Balmer series: H $\alpha$ , H $\beta$ , H $\gamma$ , H $\delta$

We applied the method presented in order to improve observability of the Balmer series spectral lines that are dominant in type A–G stars. For this purpose we chose three observational targets. First of all, we selected the star Deneb ( $\alpha$  Cygni, HD 197345, HR 7924) which is a blue-white early-type A hot supergiant (spectral type A2Ia) and its spectrum has supplied a solid anchor point by which other stars are classified (Johnson and Morgan 1953; Schiller and Przybilla 2008; Albayrak 2000). Secondly, we observed the star Procyon A ( $\alpha$  Canis Minoris, HD 61421, HR 2943) which is a young main sequence type F white sub-giant, very close to our own solar system (Kervella 2004). Lastly, we chose 16 Cygni A (HD 186408, HR 7503), which is an evolved main sequence G type star that is a solar analog, and therefore been a case study as a glance to the future of our own sun (Kovtyukh et al. 2003). Results of the observations are presented in Fig. 5(a, b and c).

The red line in each panel represents the case where the spectrum was retrieved from the full interferogram, while the black line represents the latter case of the partial interferogram where the region of path differences is optimized to correspond to each line width, in order to maximize its contribution. For proper comparison, the intensities are normalized by using a standard method of equalizing the integral below the specific wavelength range for all compared methods. The exposure times were equal in both cases.

We calculated the line depth for each spectral line in question in a very simple manner, by measuring deviation from background level between two sides of the spectral line to its lowest point. The S/B improvement was calculated by taking the ratio of line depths between the methods (partial to full interferogram). More sophisticated methods could also be used (Talbert and Edmonds 1966). Since the experiment was carried out in the visible, where fluctuating noise sources are less prominent compared to the infra-red regime, we dealt only with the contribution by the continuum. When employed in the infra-red, the standard treatment of noise will apply. A general treatment of the signal to noise ratio was already given in (Schwartz et al. 2012).

We achieved an observability improvement in the range of 4.5–35.7 and summarized the results in Table 2. Notice that the improvements vary quite significantly since they depend

**Fig. 5** Retrieved spectral Balmer series (left to right) of the stars: (a) Deneb, (b) Procyon A & (c) 16 Cygni A. The red line in each panel represents the case where the spectrum was retrieved from the full interferogram, while the black line represents the case of the partial interferogram using the same exposure time

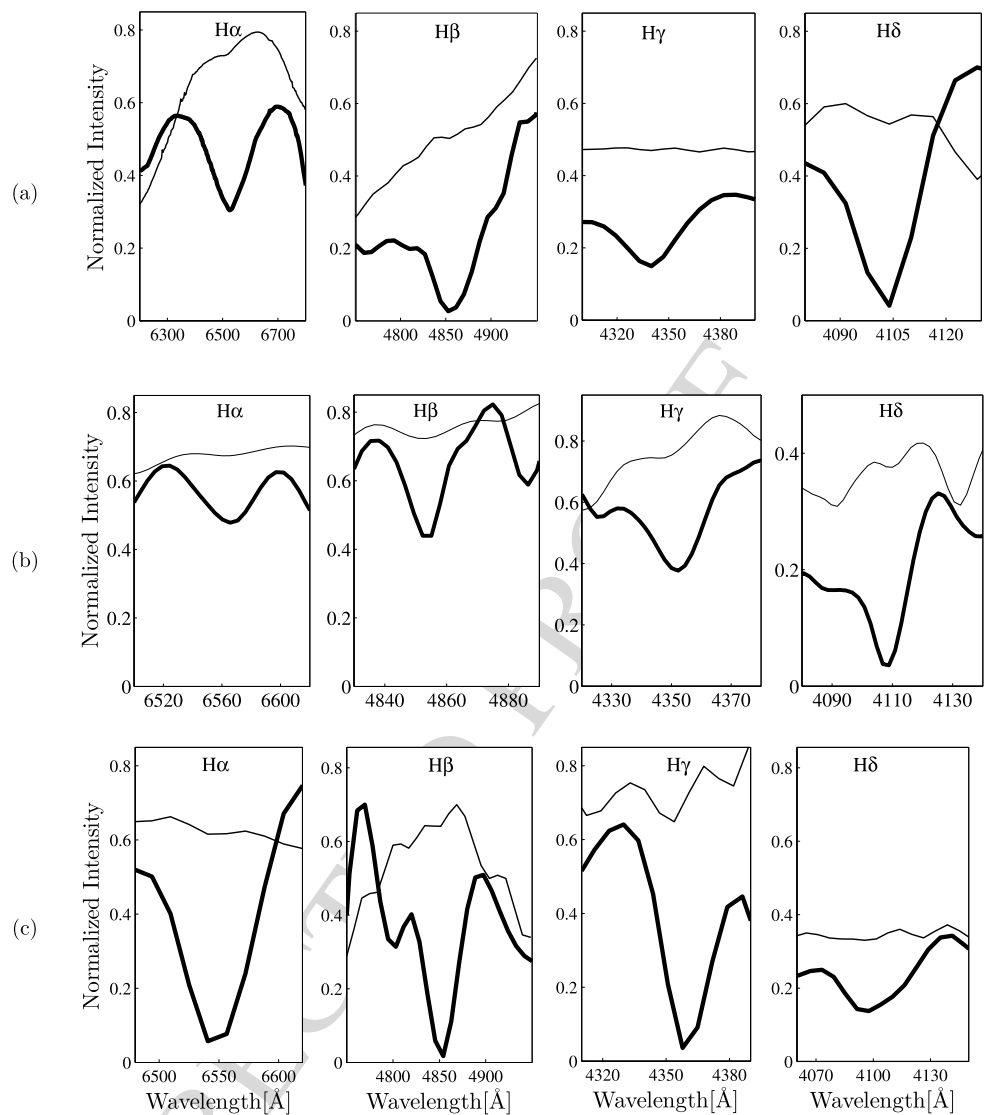


**Table 2** S/B improvement of Balmer lines when employing the partial OPD compared with the full OPD

Star	S/B Improvement				Stellar line widths range
	H $\alpha$	H $\beta$	H $\gamma$	H $\delta$	
Deneb ( $\alpha$ Cygni)	18.8	17.7	22.7	17.1	9 Å–30 Å
Procyon A ( $\alpha$ Canis Minoris)	12.8	7.1	8.5	10.3	24 Å–32 Å
16 Cygni A	22.3	12.8	4.5	35.7	4 Å–16 Å

both on the actual line depth, and on the matching of our interferometer to the line width in question. Better matching of the path differences in the partial interferogram to the chosen spectral features widths will result in a bigger improvement over all the spectral lines presented. To facilitate that, finer tuning and further development of better control of the interferometer is required and is currently in progress. However, we cannot always estimate an exact width of a spectral feature but rather a range of widths which represents a more realistic scenario where the spectrum sought is

unknown. This will optimally improve a specific line width and will be less effective to the rest. This fact will result in a bigger variance of S/B improvements as manifested in Table 2.

## 2.2 Other atomic and molecular lines (Ca II, Na I, Mg I, Fe I, He I, TiO, ZrO)

Following the above results, we extended the observations to improve observability of more elaborate spectral features

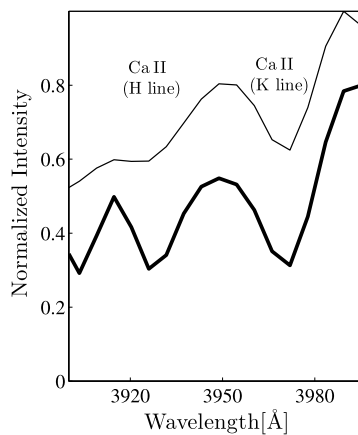


**Fig. 6** Retrieved spectral calcium K and H lines of the star 16 Cygni A. Spectral lines are formatted as in Fig. 5

for cooler stars along with a case of a low apparent magnitude, extremely hot blue star. The stars chosen for this analysis were from spectral types G, K, B, M and S. The first of these was 16 Cygni A, for which we already have analyzed its Balmer series. This time we focused on improving the observability of the ionized calcium lines in the blue edge of the visible spectrum (H and K lines) (Kramida et al. 2013) with line widths of  $\sim 15$  Å (Kaler 1989). In Fig. 6, the retrieved Ca II lines are shown for the case of full interferogram (red) and for partial interferogram (black). The observability improvements were 5.74 for the K line (3930 Å) and 2.2 for the H line (3970 Å).

Secondly, we chose Aldebaran ( $\alpha$  Tauri, HD 29139, HR 1457) which is a K type orange giant star that veered off the main sequence line of the Hertzsprung–Russell diagram (Thomas 2005). For this we chose to focus on magnesium (Mg I, 5170 Å, line width  $\sim 40$  Å) and sodium (Na I, 5890 Å, doublet line width  $\sim 20$  Å) lines as shown in Fig. 7 (Montes et al. 1999). The retrieved lines are again presented for the case of full interferogram (red) and for partial interferogram (black). The observability improvements here were 13.4 for the Mg I line and 4.5 for the Na I line.

Thirdly, we chose the spectroscopic standard star, BD+25°3491, which is a B type main sequence blue star with apparent magnitude of 10.47 in the V-band and has prominent neutral helium lines (He I) in the blue region of the spectrum<sup>1</sup> (Stone 1977; Jacoby et al. 1984; Saad and Nouh 2011). In this case, we center on two neutral helium lines at wavelengths 4147 Å (line width  $\sim 11$  Å) and 4471 Å (line width  $\sim 20$  Å) as shown in Fig. 8. The retrieved lines are displayed in the same form as in Figs. 6 and 7. The observability improvements for this object were 18.1 for the first line (left) and 5.7 for the latter (right).

<sup>1</sup><http://www.naoj.org/Observing/Instruments/FOCAS/Detail/UsersGuide/Observing/StandardStar/Spec/SpecStandard.html>.

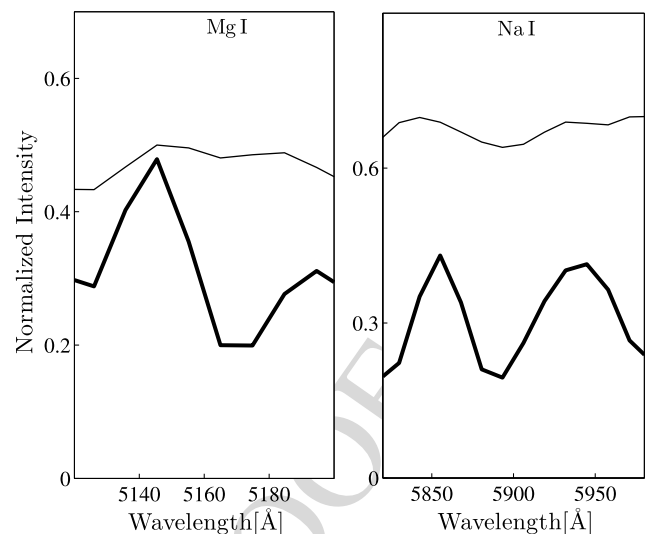


**Fig. 7** Retrieved spectral magnesium and sodium lines of the star Aldebaran. *Left to right*: Mg I, Na I lines. Spectral lines are formatted as in Fig. 5

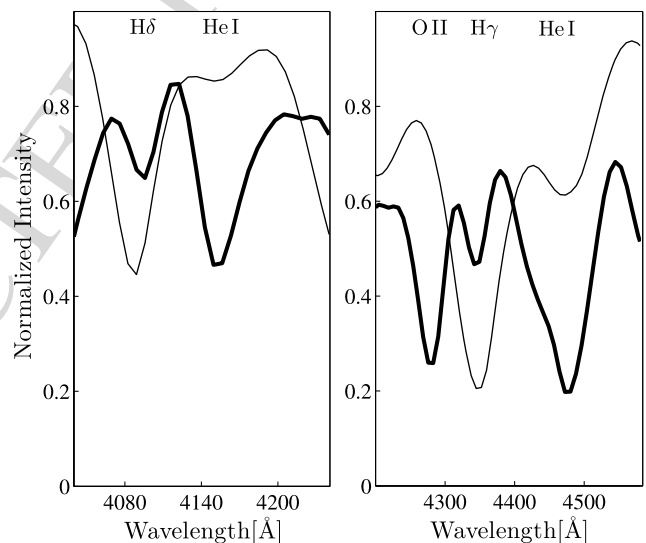


**Fig. 8** Retrieved neutral helium lines (He I) of the star BD+25°3491. Spectral lines are formatted as in Fig. 5. *Right panel*: a prominent O II absorption line appears in the partial interferogram spectrum but is absent in the full interferogram case

Furthermore, while studying the partial interferogram spectrum in the H $\gamma$  region (right panel), an unexpected prominent absorption line appeared which was later identified as an O II line at 4275 Å region (Struve 1931; Kurucz and Bell 1995). This example distinctly demonstrated how the partial interferogram method far surpasses the regular full FTS method. Moreover, it is also clearly noticeable that the H $\gamma$  and H $\delta$  (line widths  $\sim 40$  Å) spectral lines (Saad and Nouh 2011) were scaled down in the partial interferogram case, due to the fact that their line widths do not match those

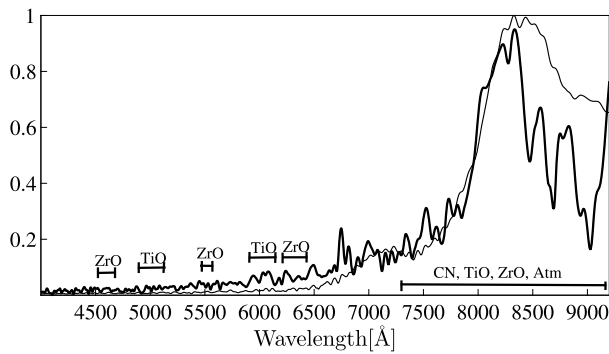


**Fig. 9** R Andromedae multiple spectral features (mainly TiO, ZrO and some Earth atmospheric absorption lines). Spectral lines are formatted as in Fig. 5

of the He I lines and are not optimized for the chosen path differences.

Finally, we obtained the interferograms of the star R Andromedae (HD 1967, HR 90) and of Betelgeuse ( $\alpha$  Orionis, HD 39801, HR 2061). R Andromedae is a Mira-type variable star with a spectral class of type S, as it shows mostly molecular absorption bands of zirconium monoxide (ZrO) and of titanium monoxide (TiO) in its spectrum (Aller and Keenan 1951; Baxandall 1924; Keenan and Boeshaar 1980; Keenan et al. 1954, 1974; Merrill 1922, 1947, 1952; Merrill and Greenstein 1956). Betelgeuse is one of the famous type M red supergiants which shows, amongst others, lines belonging to oxide molecules, in particular, titanium monoxide (TiO) (Valenti 1998; Martell et al. 2008; Swings and Struve 1932).

For these two stellar objects, we present in Figs. 9 and 10 the complete spectrum retrieved from the full interferogram (red, marked central) and from the partial interferogram (black).

In Fig. 10, the two black lines (marked partial 1&2) are spectra from different data sets (checked for repeatability) that were obtained from the case of partial interferogram using the same exposure time and path differences. Considering these last stars, the path differences for the partial case were chosen so that the delicate complex nature of molecular features in the spectrum will be optimally enhanced. This clearly shows the increased detection of finer details in the spectra of both stellar objects.

### 2.3 Further verification and comparison

In the final stage of this work we present two more observational results in which we used a standard grating spectrometer on the Wise 1m telescope<sup>2</sup> in order to verify the results presented in the previous sections. For that purpose,

<sup>2</sup>[http://wise-obs.tau.ac.il/wise\\_ins.html](http://wise-obs.tau.ac.il/wise_ins.html).

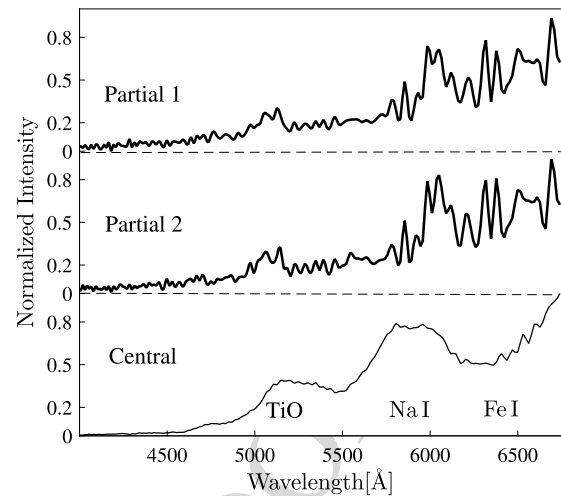


**Fig. 10** Retrieved spectrum of the star Betelgeuse. Examples of TiO, NaI, FeI lines. The red line (marked: central) represents the case where the spectrum was retrieved from the full interferogram, while the black lines (marked: partial 1&2) represent the case of the partial interferogram using the same exposure time for two different data sets (checked for repeatability) with the same path differences

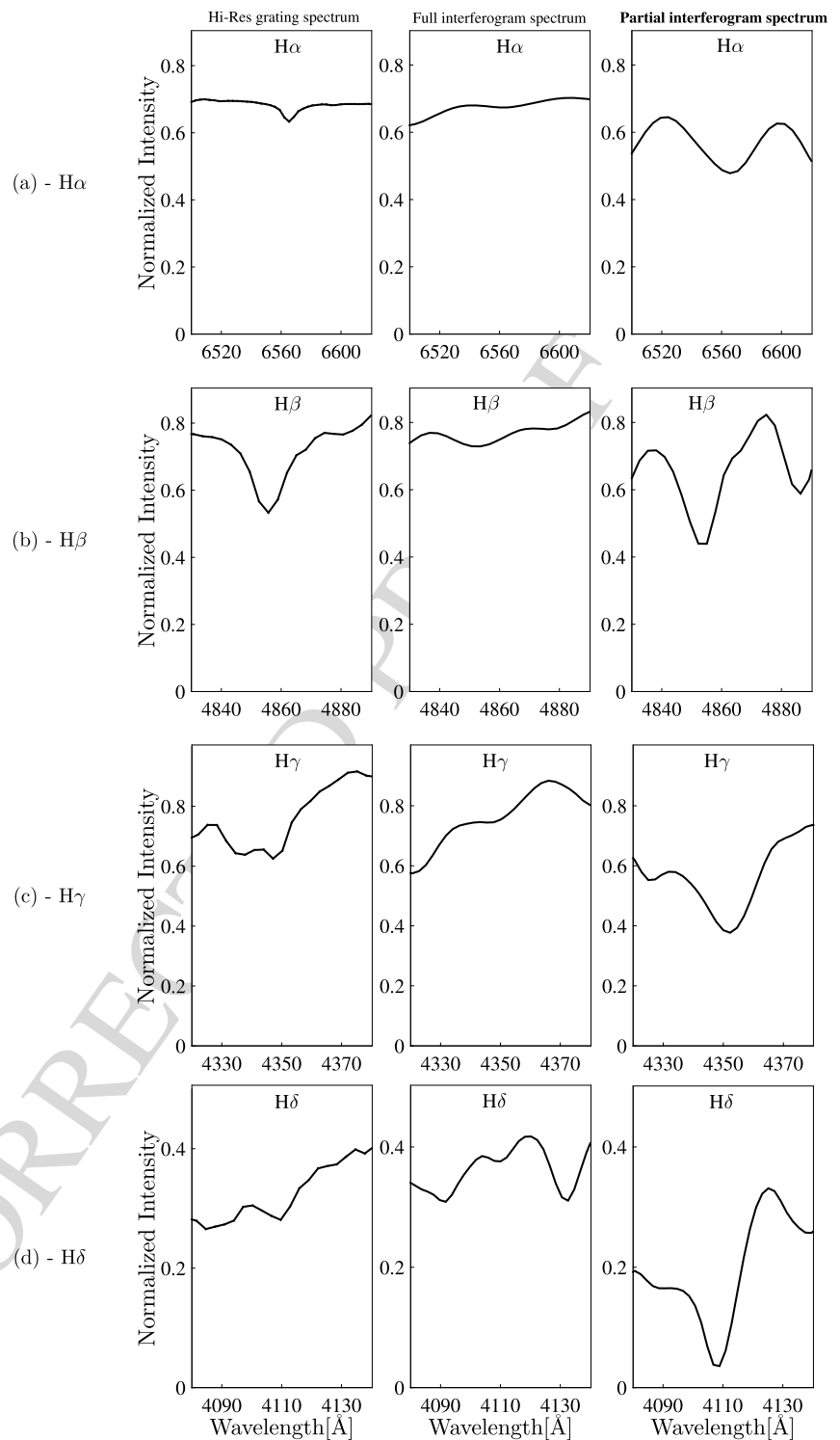
we chose two stars from Table 1 and obtained their spectra with approximately similar conditions (airmass, exposure times). In Figs. 11 and 12 we present spectral lines in the stars Procyon A (Balmer lines) and Betelgeuse (TiO—band width  $\sim 15 \text{ \AA}$ , Na I—doublet line width  $\sim 15 \text{ \AA}$ , Fe I—line width  $\sim 20 \text{ \AA}$ ) (Lobel 2011). The three panels (left to right) in each sub figure represent the cases of higher resolution ( $R \sim 1300$ ) echelle grating spectrograph as well as the spectrum retrieved from full and partial interferogram, previously presented in Figs. 5(b) and 10.

This form of Fourier transform spectroscopy, with no moving parts, was limited in resolution by pixelization of the aperture image on the CCD to  $R \sim 400$ . This is obvious from the  $H\alpha$  line as shown in Fig. 11(a). Figure 12, as in Fig. 11, is supplemented with an additional data set, as formerly explained.

For comparison between the different methods, i.e. a grating spectrometer and partial interferogram, we calculated the observability enhancement for each spectral feature in question and summarized the results in Table 3. We achieved an S/B improvement in the range of 1.5–7.9 for these spectral lines. One can appreciate from Fig. 11(b) that when the line itself has width about  $\delta k$  (optimum), there is little improvement while the resolution is reduced as expected. Additionally, our method could also be implemented as a post-processing technique to any spectroscopic method at the expense of amplifying the noise as well.

Therefore, we compared the real time partial interferogram spectrum to the high resolution grating spectrum, to which we applied a post-processing band-pass Fourier filter, as similar as possible to the partial interferogram method

**Fig. 11** Improving observability of the Balmer series of Procyon A. The three columns (*left to right*) represent the cases of high resolution grating spectrometer (*blue*) as well as the spectra retrieved from full (*red*) and partial (*black*) interferograms. Data was obtained under similar conditions and exposure time



(thus removing the continuum part of the spectrum and rejecting the unwanted spectral lines widths). The comparison results are shown in Figs. 13 and 14, where in each plot the black line is the real time partial interferogram spectrum while the blue line is the similarly post-processing filtered grating spectrum. Figure 14, as in Fig. 13, is supplemented

with an additional data set (for partial interferogram) as formerly explained. From Figs. 13 and 14, one can see that the observability of the spectra is almost matched for both methods, with a slight advantage to the partial interferogram method in some cases (up to a factor of 2, although with clearly degraded resolution).

**Fig. 12** Improving observability of TiO, Na I, Fe I lines in the retrieved spectrum of the star Betelgeuse. The three columns (*left to right*) represent the cases of high resolution grating spectrometer (*blue*) as well as the spectrum retrieved from the full interferogram (*red*) and from partial interferogram (*black*), for which we used the same parameters for two different data sets (checked for repeatability)

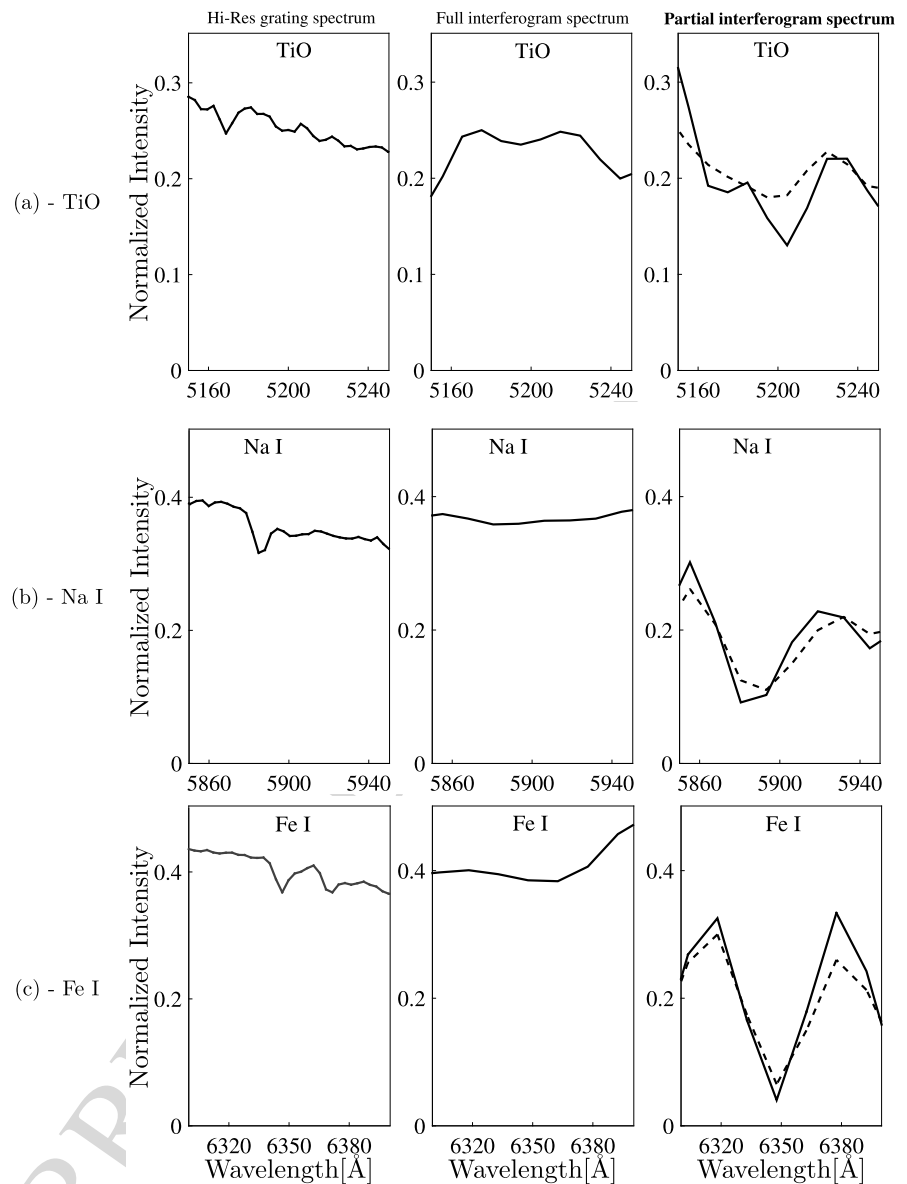


**Table 3** Improvement in the S/B for different spectral features for partial interferogram relative to a grating spectrometer

Star	Spectral line	S/B improvement	Line widths
Procyon A ( $\alpha$ Canis Minoris)	H $\alpha$	3.2	25 Å
	H $\beta$	1.5	32 Å
	H $\gamma$	3.3	27 Å
	H $\delta$	5.8	24 Å
Betelgeuse ( $\alpha$ Orionis)	TiO	7.9	15 Å
	NaI	3.7	15 Å
	FeI	6.5	20 Å

The reason for this near match is that the central wavelengths in question were known in advance, thus increasing the effectiveness of the grating spectra S/B. This is even though originally the collected light was dispersed over

more measurement channels (higher resolution) and therefore a lower S/B. In the more realistic case where only a range of band widths in the light source spectrum could be pre-assessed, the partial interferogram method would have a

**Fig. 13** Comparison between partial interferogram (*black*) and post-processed filtered high resolution grating spectrometer (*blue*), of the Balmer series spectral lines of Procyon A. Data were obtained under similar conditions and exposure time

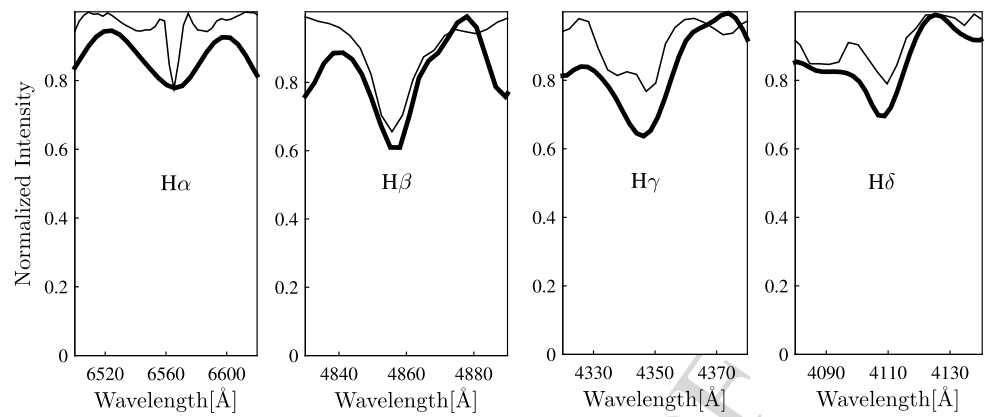
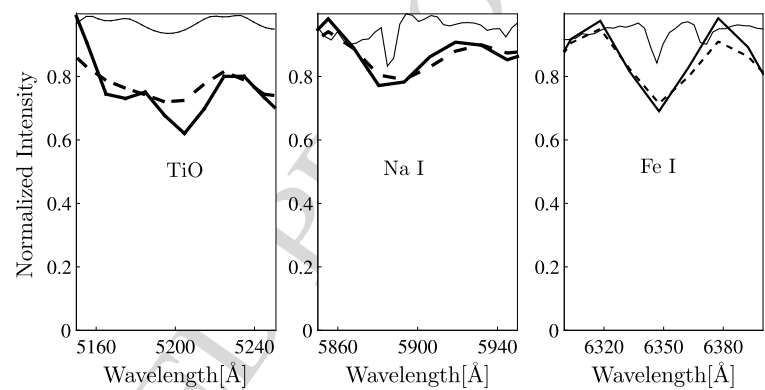


**Fig. 14** Comparison between partial interferogram (*black solid and dashed lines*—two different data sets, checked for repeatability) and post-processed filtered high resolution grating spectrometer (*blue*), of the TiO, Na I, Fe I spectral lines of the star Betelgeuse. Data were obtained under similar conditions and exposure time



significant advantage since the same amount of light would be accumulated in a smaller number of measurement channels thus increasing S/B over that of a post-processed filtered higher resolution grating spectrum, as explained in the introduction section.

### 3 Discussion and conclusions

We presented the results of an observation series designed to demonstrate an interferometric method to improve observability of spectral features in an overwhelming background of continuum and other spectral lines with different widths. Following the results presented, we now propose two examples of problems in observational astronomy and astrophysics to which this method could contribute. Clearly, applications in other areas of physics abound.

The first is the determination of the mass of supermassive black holes associated with active galactic nuclei in galaxies. This physical parameter is essential for an in-depth understanding of the mechanism powering AGNs and their role in galaxy evolution (Peterson et al. 2004). One of the methods used for this purpose is reverberation mapping (RM) in which a series of spectra of the AGN is obtained over a long period of time (months to years) in an attempt to resolve the reverberation time lag between a change in con-

tinuum emission from an accretion disk and the delayed response due to light travel time of spectral line emission from high velocity clouds in a distant broad-line region (BLR) (Peterson et al. 2004; Rafter et al. 2011). The broad optical emission lines come from material close to the central black hole. The lines are broad because the emitting material is revolving around the black hole at high speed causing a range of Doppler shifts of the emitted photons.

In RM analysis, a problem resides in the fact that it is difficult to differentiate the flux variability of the hydrogen emission lines from the BLR, from that of the strong continuum when attempting to construct the light curve of the BLR. Another problem emerges when estimating the radial velocity (that is, the mass of the black hole) using the widths of the BLR spectral lines. In this scrutiny, narrow optical emission lines, which come from more distant cold material, need to be fitted out in order to correctly assess the broad lines widths in the spectrum. Consequently, the interferometric method we presented in this paper could improve the RM analysis and outcomes when handling these obstacles.

A second example, which was the initial impetus for this work (Schwartz et al. 2012), is to use this method in detection of faint spectral signals originating from exoplanets. The problem is that an Earth-like extra-solar planet is expected to reflect a luminosity which is many orders of magnitude less than that of the parent star. Therefore by looking

at an off-center part of an interferogram received by Fourier transform spectrometer in the infra-red, we could identify spectral lines in light collected from such a planet. This can result in superior sensitivity to narrow spectral bands (such as complex molecular features), which are expected in the planet spectrum, but are absent in the parent star (Schwartz et al. 2012).

In summary, we presented the results of an observational campaign which supports the proposed method of emphasizing spectral features in the presence of a strong background by optimized sampling of their Fourier interferograms. We showed that with a proper selection of region of path lengths we were able to considerably improve the observability of weak spectral features in different stellar spectra. This method could be applicable to different aspects of spectroscopic astronomical observations such as: identification of complex molecular features in Earth-like exoplanets search and spectral analysis of AGNs for velocity measurement in light of temperature broadening effects, in order to determine some of their more important physical parameters, which are essential for a deeper understanding of the AGNs and the galactic dynamics over time.

**Acknowledgements** We are grateful for experimental assistance and inputs from Dr. Shai Kaspi, Dr. Stephen Rafter and S. Hoida. E.S. acknowledges financial support from the Asher Space Institute at Technion. Parts of this work were supported by the Israel Science Foundation and the Ministry of Science and the Minerva Center for Non-Linear Dynamics. This work was done based on observations obtained with the Tel Aviv University Wise Observatory 1 m telescope.

## References

- Albayrak, B.: *Astron. Astrophys.* **364**, 237 (2000)
- Aller, L.H., Keenan, P.C.: *Astrophys. J.* **113**, 72 (1951)
- Baxandall, F.E.: *Mon. Not. R. Astron. Soc.* **84**, 568 (1924)
- Bell, R.J.: *Introductory Fourier Transform Spectroscopy*. Academic Press, New York (1972)
- Chesneau, O., et al.: *Astron. Astrophys.* **521**, A5 (2010)
- Ferrari, G., et al.: *Adv. Exp. Med. Biol.* **191**, 873 (1985)
- Grieco, G., et al.: *Appl. Opt.* **50**, 4516 (2011)
- Hardorp, J., Tomkin, J.: *Astron. Astrophys.* **127**, 277 (1983)
- Hearnshaw, J.B.: *The Analysis of Starlight: One Hundred and Fifty Years of Astronomical Spectroscopy*. Cambridge University Press, Cambridge (1986)
- Jacoby, G.H., et al.: *Astrophys. J. Suppl. Ser.* **56**, 257 (1984)
- Jaschek, C., Jaschek, M.: *The Behavior of Chemical Elements in Stars*. Cambridge University Press, Cambridge (1995)
- Johnson, H.L., Morgan, W.W.: *Astrophys. J.* **117**, 313 (1953)
- Kaler, J.B.: *Stars and Their Spectra: An Introduction to the Spectral Sequence*. Cambridge University Press, Cambridge (1989)
- Kaufer, A., et al.: *Astron. Astrophys.* **305**, 887 (1996)
- Keenan, P.C., Boeshaar, P.C.: *Astrophys. J. Suppl. Ser.* **43**, 379 (1980)
- Keenan, P.C., et al.: *Astrophys. J.* **120**, 484 (1954)
- Keenan, P.C., et al.: *Astrophys. J. Suppl. Ser.* **28**, 271 (1974)
- Kervella, P.: *Astron. Astrophys.* **413**, 251 (2004)
- Kovtyukh, V.V., et al.: *Astron. Astrophys.* **411**, 559 (2003)
- Kramida, A., et al.: *NIST Atomic Spectra Database (ver. 5.1)*. National Institute of Standards and Technology, Gaithersburg (2013). <http://physics.nist.gov/asd> [2014, May 17]
- Kurucz, R.L., Bell, B.: *Atomic Line Data (R.L. Kurucz and B. Bell) Kurucz CD-ROM No. 23*. Smithsonian Astrophysical Observatory, Cambridge (1995)
- Kyle, T.G.: *Appl. Opt.* **16**, 326 (1977)
- Lipson, A., et al.: *Optical Physics*, 4th edn. University Press, Cambridge (2011)
- Lobel, A.: *Can. J. Phys.* **89**, 395 (2011)
- Lovis, C., Fischer, D.A.: *Radial velocity techniques for exoplanets*. In: Seager, S. (ed.) *Exoplanets*. University of Arizona Press, Tucson (2010), 31 pp.
- Martell, S.L., et al.: *Publ. Astron. Soc. Pac.* **120**, 839 (2008)
- Merrill, P.W.: *Astrophys. J.* **56**, 457 (1922)
- Merrill, P.W.: *Astrophys. J.* **105**, 360 (1947)
- Merrill, P.W.: *Astrophys. J.* **116**, 21 (1952)
- Merrill, P.W., Greenstein, J.L.: *Astrophys. J. Suppl. Ser.* **19**, 225 (1956)
- Montes, D., et al.: *Astrophys. J. Suppl. Ser.* **123**, 283 (1999)
- Pecaut, M.J., Mamajek, E.E.: *Astrophys. J. Suppl. Ser.* **208**, 9 (2013)
- Perrin, M.N., Spite, M.: *Astron. Astrophys.* **94**, 207 (1981)
- Peterson, B.M., et al.: *Astrophys. J.* **613**, 682 (2004)
- Prieto, A.C., et al.: *Astrophys. J.* **567**, 544 (2002)
- Rafter, S.E., et al.: *Astrophys. J.* **741**, 66 (2011)
- Ribak, E.N.: *Proc. SPIE* **6268**, 62683G (2006), *Advances in Stellar Interferometry*
- Ribak, E., Leibowitz, E.: *Appl. Opt.* **24**, 3088 (1985)
- Ribak, E., Lipson, S.G.: *Appl. Opt.* **20**, 1102 (1981)
- Ribak, E., et al.: *Appl. Opt.* **24**, 3094 (1985)
- Rodgers, C.D.: *Inverse Methods for Atmospheric Sounding: Theory and Practice*. World Scientific, Singapore (2000)
- Saad, S., Nouh, M.: *Int. J. Astron. Astrophys.* **1**, 45–51 (2011)
- Schiller, F., Przybilla, N.: *Astron. Astrophys.* **479**, 849 (2008)
- Schwartz, E.: *Astronomical observations of remote planets*. PhD thesis, Technion—Israel Institute of Technology. <http://ezfind.technion.ac.il/vufind/Record/002368275> (2014)
- Schwartz, E., et al.: *Astron. J.* **144**, 71 (2012)
- Stone, R.P.S.: *Astrophys. J.* **218**, 767 (1977)
- Struve, O.: *Astrophys. J.* **74**, 225 (1931)
- Swings, P., Struve, O.: *Phys. Rev.* **39**, 142 (1932)
- Talbert, F.D., Edmonds, F.N., Jr.: *Astrophys. J.* **146**, 177 (1966)
- Thomas, R.A.: *Astrophys. J.* **618**, 493 (2005)
- Valenti, J.A.: *Astrophys. J.* **498**, 851 (1998)